# Low Volume Gas-Flow Seeding for Highly Resolved Velocimetry of the Boundary Layer

Christoph Möller<sup>1,\*</sup>, Christopher Geschwindner<sup>1</sup>, Andreas Dreizler<sup>1</sup>

1: Technical University of Darmstadt, Department of Mechanical Engineering, Reactive Flows and Diagnostics, Otto-Berndt-Str. 3, 64287 Darmstadt, Germany \*Corresponding author: moeller@rsm.tu-darmstadt.de

Keywords: PIV particle seeding, Fire research, Boundary layer flows, Particle image velcimetry, Particle tracking velocimetry.

#### **ABSTRACT**

Ensuring fire safety in polymeric materials, which are inherently flammable but widely used in various industries, is of significant societal and economic importance. This study is part of a broader effort to understand polymer combustion and flame retardant effectiveness at a fundamental level. A major focus is the behavior of polymers burning along a vertical wall, a configuration chosen to study the release of flammable gases during pyrolysis, which contributes to the self-sustaining combustion reaction of a fire. This process occurs predominantly near the polymer surface within the boundary layer, requiring detailed analysis to evaluate flame retardant effectiveness. Our experimental setup replicates polymer pyrolysis using a flame-wall interaction burner with a vertical jet and a small inlet to mimic the release of flammable gases. The primary challenge in this setup is the introduction of seeding particles for Particle Image Velocimetry (PIV) measurements at low volume flow rates, which is complicated by reflections from the wall and the small flow scale relative to the main flow. To address this problem, we have developed a novel piezo-based ultrasonic seeder capable of controlled seeding at extremely low flow rates, thereby improving the accuracy of PIV measurements in non-reactive configurations. This seeder uses a piezo ring to excite a perforated metal membrane, forming uniform aerosol droplets. The design ensures a steady supply of particles, which is critical for evaluating boundary layer conditions. Our results demonstrate the seeder's ability to maintain sufficient seeding density in the low volume flow region, facilitating detailed velocimetry analysis. The innovative seeder design proves effective in overcoming the limitations of conventional methods and provides new insights into polymer combustion processes and the role of flame retardants.

### 1. Introduction

Fire safety is a critical concern for polymeric materials, which are highly flammable yet widely used in various industrial applications and daily life (Velencoso et al., 2018; Schartel, 2021; Dasari et al., 2013; Geschwindner et al., 2023). The study of flame retardants for polymers and fire propagation is thus of significant societal and economic importance. This work is part of a project aimed

at understanding polymer combustion and the effect of flame retardants at a fundamental level, with a particular focus on the behaviour of polymers burning along a vertical wall.

The vertical configuration for polymer combustion serves as a basic generic case to study the release of flammable gases during pyrolysis that contribute to the self-sustaining combustion reaction of a fire. This process occurs primarily near the polymer surface, within the boundary layer, where the interaction between the flame retardant and the pyrolysis products of the polymer is most critical. Understanding this process is critical for evaluating the effectiveness of flame retardants, which has been investigated in previous numerical studies (Steinhausen et al., 2023) and is currently subject of experimental investigation.

An analogous system mimicking this vertically oriented polymer combustion scenario has been designed based on a flame-wall interaction burner, whose basic design is well-documented in the literature (Zentgraf, 2022; Zentgraf et al., 2024; Greifenstein et al., 2024). In this setup, a vertical jet from a converging square nozzle approaches a vertical wall from below. For the adapted design, fuel (CH<sub>4</sub>) is introduced from an active wall through a 20 mm wide by 1 mm high inlet to mimic the release of flammable gases during pyrolysis of polymeric materials. The inlet flow is specified as a small fraction of the bulk mass flux per area from the main nozzle, resulting in flow rates between 2.579 L/h and 10.32 L/h.

A starting point of the study is to characterize the inflow boundary conditions and the influence of the active wall inlet on the boundary layer, starting with the non-reactive flow as a reference. Therefore, Particle Image Velocimetry (PIV) is used to measure the velocity profile up to the boundary layer and near the inlet. However, seeding the flow through the inlet with a sufficient number of particles has proven to be a significant challenge due to the low volume flow rates.

To overcome the limitations of conventional seeders designed for much higher volume flow rates, this work presents a newly developed piezo-based seeder for liquids capable of controlled seeding of tracer particles at extremely low flow rates in non-reactive configurations. The seeder can effectively operate at rates well below 2.579 L/h enabling successful and accurate velocity measurements.

Section 2 describes the experimental setup for flow velocimetry applied to the generic burner system, followed by a detailed explanation of the seeder design. In the fourth section, the performance of the piezo-based seeder is analyzed and discussed. Finally, the results of the velocity measurements are presented to demonstrate the capabilities and applications of this innovative seeding technology.

# 2. Experimental Setup

The experimental setup for investigating the boundary layer flame (BLF) along a vertically oriented active wall is based on the flame-wall interaction burner described by Zentgraf (2022) and shown in Figure 1. This adaptation of the setup aims to mimic the release of flammable gases during pyrolysis of polymers.

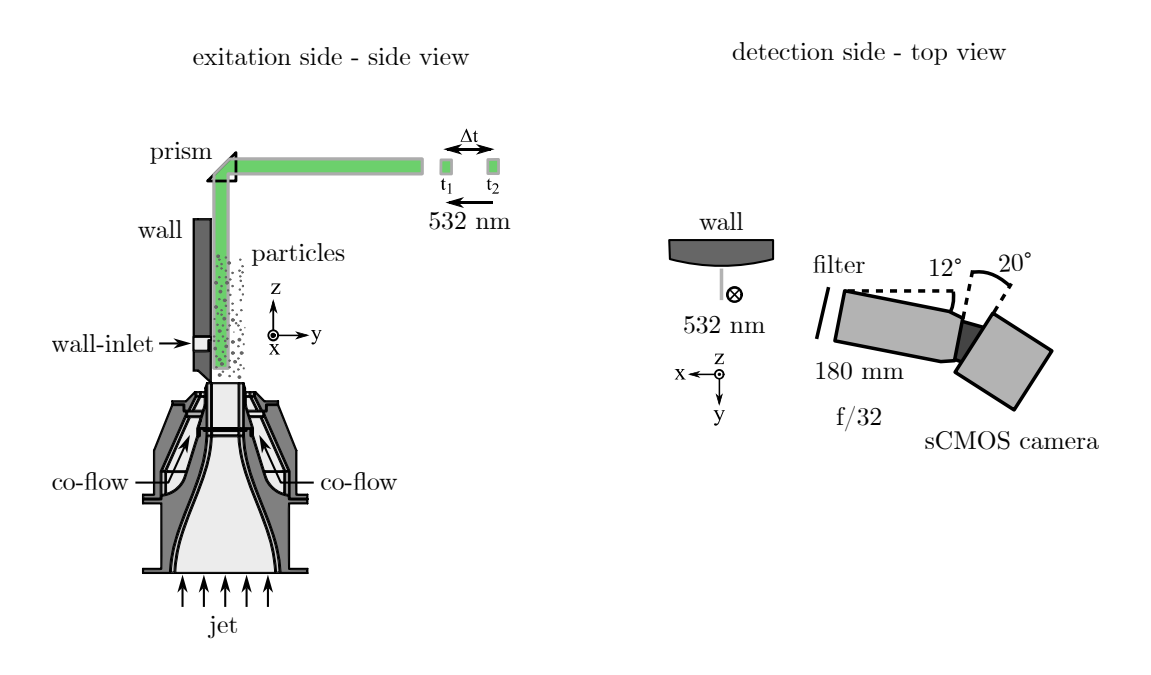


**Figure 1.** Flow configuration and schematic PIV setup with a side view of the laser exitation (left) corresponding to the perspective of Fig. 3 and a top view (right) for the detection assembly using a Scheimpflug setup. The coordinate systems indicate the directions used in this work. The origin of the coordinate system is located at the center of the top edge of the wall-inlet.

For studying the flow near the wall for chemically non-reacting conditions, the main flow setup for this work features a vertically oriented laminar jet of nitrogen surrounded by a co-flow of air. As depicted on the left side of Fig. 1, the jet exits through a contoured (Morel) nozzle with dimensions of 40 mm x 40 mm, achieving a velocity profile close to a top-hat shape with a peak axial velocity of about 2.5 m/s as previously described by Zentgraf (2022). The jet's calculated bulk velocity is about 2.24 m/s, corresponding to a Reynolds number of approximately 6150, considering a hydraulic diameter of 41.7mm and the kinematic viscosity of nitrogen at room temperature. Fuel (CH<sub>4</sub>) is introduced through a 20 mm wide and 1 mm high inlet to mimic the release of flammable gases from the wall during pyrolysis. The inlet flow rates range from 2.579 L/h to 10.32 L/h. They are specified as a small fraction of the bulk mass flux per area from the main nozzle ( $p = (\dot{m}_i/A_i)/(\dot{m}_m/A_m)$  with p = 1% or p = 4%) to describe the influence of the volume flow at the wall inlet independently from the gas temperature. This results in a calcualted horizontal velocity of  $0.036\,m/s$  at the inlet for the 1% case and  $0.14\,m/s$  for the 4% case.

Seeding particles are introduced into the flow to enable particle image velocimetry (PIV). The main jet flow is seeded using an AGF 10.0 atomizer by PALAS GmbH, which is specified to disperse Di-Ethyl-Hexyl-Sebacat (DEHS) particles with a mean droplet size of approximately 0.5 µm. Seeding the separate low-volume active wall inlet flow proved challenging, leading to the development of a novel piezo-based liquid seeder, the design of which is outlined in the following section.

The particles in the flow are illuminated by a Spitlight PIV 600 double-cavity laser at 532 nm by InnoLas Laser GmbH. The laser beam is expanded with spherical lenses (f = -50 mm and f = +250 mm) and focused to a 180  $\mu$ m thick sheet using an f = +750 mm lens. A prism redirects the laser sheet downwards into the probe volume, creating a nearly parallel but slightly angled 10 mm wide sheet approaching the wall. The Mie-scattering from the particles is captured using an Imager sCMOS camera by LaVision GmbH with a 180 mm macro lens at f/32. It is equipped with a bandpass filter of  $532 \pm 10 \, nm$  to suppress background radiation. The camera and lens are positioned at a 20° angle with a Scheimpflug setup to prevent vignetting close to the wall while ensuring the entire laser sheet is in focus (see Fig. 1 on the right). Images are dewarped using DaVis 10.2.1 by LaVision, resulting in a projected pixel size of approx. 6 µm, with a field of view of 13 mm normal and 16 mm parallel to the wall. Despite the shallow angle between the laser sheet and the wall, light reflections from the incident laser sheet pose a significant challenge to imaging particles in the boundary layer region. To avoid oversaturating the camera, we had to significantly reduce the laser intensity. However, this reduction in laser intensity reduced the dynamic range of the particle images, resulting in a noticeable stripey noise pattern from the camera. This resulted in the stripe pattern visible in the averaged images shown below.

This comprehensive experimental setup provides the basis for a detailed analysis of the inlet boundary conditions. It effectively mimics pyrolysis during polymer combustion and allows a thorough investigation of flame retardant effectiveness. In particular, the pyrolysis of polymers involves a very small flow compared to the main flow, which poses a significant challenge to the PIV equipment beyond reflections from the wall. This motivated the design of a new seeder as described in the next section.

## 3. Piezo-Based Ultrasonic Seeder Design

The design of the piezo-based or, more generally, vibration-based seeder was inspired by aerosol generation techniques used in shock tube studies, such as those demonstrated by Haylett et al. in 2012 (Haylett et al., 2012). Three system designs for vibration-based aerosol generation were considered in this work.

In the submerged ultrasonic design, a piezo disk vibrates at its resonant frequency at a specific distance below the liquid surface. The pressure waves are focused at the surface, causing the surface to break into droplets, as used for particle-based velocimetry by Haylett et al. Haylett et

al. (2012). However, testing of this design revealed flow fluctuations during extended seeder run times, likely due to intermittent large droplets and occasional clogging by liquid accumulation.

Another method considered was surface acoustic wave aerosol generation, in which an acoustic wave breaks the liquid on a thinly wetted surface into droplets, originally described by Kurosawa et al. (1995). Despite ongoing research in this area, such as that of Roudini et al. (2024), this method was deemed unsuitable for the current work.

Finally, we successfully utilized the membrane-based aerosol generation technique commonly found in commercially available inhalable drug devices and fragrance dispensers. This technique has been well documented and characterized in several studies, such as that of Wedding (1975). In these devices, a piezo ring excites a thin perforated metal membrane at its resonant frequency. As the membrane oscillates, it pushes the adjacent liquid through the perforations, forming tiny aerosol droplets on the other side.

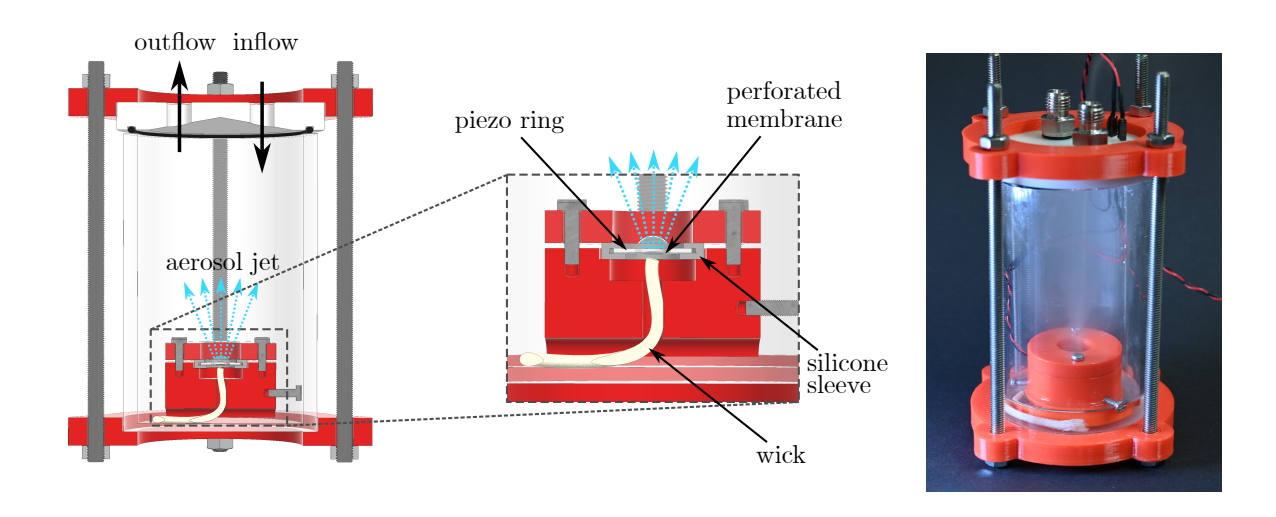


**Figure 2.** Schematic (left) and photo (right) of the seeder built in this work. The aerosol generator is placed inside a sealed flask with controlled inflow. The aerosol generator is shown in more detail in the center, indicating the thin perforated metal membrane, with the attached piezo ring on top of the wick drawing in fresh ethanol.

Figure 2 illustrates the design and construction of the piezo-based ultrasonic seeder. The schematic on the left shows the overall setup, where the aerosol generator is housed in a sealed flask with controlled inflow and outflow. The middle panel provides a close-up view of the aerosol generator, highlighting the thin perforated metal membrane and the piezo ring. The wick mechanism provides a continuous supply of liquid ethanol to the membrane, promoting uniform atomization. The photo on the right shows the actual seeder apparatus used in our experiments.

For this work, the membrane and piezo ring combination was obtained from a commercial groove

water atomization kit. An oil lantern wick continuously supplies liquid to the membrane from below, ensuring consistent atomization. The atomization system is housed in a flask, with the liquid reservoir located at the bottom. The gas flow enters and exits the flask at the top, facilitating the transport of seeded particles to the inlet, located approximately 20 cm downstream of the seeder flask. The piezo ring is driven by a 60 V peak-to-peak signal at a frequency of approximately 108 kHz, which is closely tuned to the membrane's resonance. This design ensured a steady supply of seeding particles, which is critical for low volume flow PIV measurements. Using ethanol as the seeding liquid, the piezo seeder enabled seeding for PIV at volume flows below 2.579 Ln/h. An evaluation of the performance of the seeder is discussed in the next section.

#### 4. Results & Discussion

### 4.1. Seeder Performance

Four cases were compared to evaluate the performance of the piezo-seeder designed in this work. Cases (a) and (b) are operated with the wall-inlet set at 1% of the mass flux per area of the main jet, while (c) and (d) are at 4%. Sets of 200 double-frames for PIV were recorded with (case (b) and (d)) and without (case (a) and (c)) the piezo-seeder for the wall inlet turned on to compare the results at each percentage. The images of the Mie-scattering were then processed using DaVis 10.2.1; processed Mie-scattering images are shown in Fig. 3. Firstly, a background, which included reflections from the wall, was subtracted. The reflections, as well as the stripey background pattern, varied slightly between each frame. Then, the intensity was homogenised using a sliding min-max filter with a window length of 3 pixels (Adrian & Westerweel, 2011). Despite the short window length, this proved effective at homogenising the particles visible in the flow. The window length was chosen to avoid the influence of the reflections over a large area of the image. Lastly, the images were dewarped based on target images to account for the distortion caused by the lens and the Scheimpflug adapter.

Fig. 3 shows a small section of the entire recorded field of view, with the main jet oriented upwards and the wall on the left. Imperfections of the wall surface cause significant reflections at the wall, 0.5 mm above the inlet and in the region at z = 1.5 mm. The seeding of the main jet appears spatially homogeneous in the entire field of view upstream of the wall-inlet. Downstream of the wall-inlet cases (a) and (c) with the piezo-seeder turned off, as expected, show an absence of particles close to the wall. Due to the higher inflow rates in case (c), there are almost no particles in the region up to y = 0.5 mm from the wall, while in case (a), only the area up to about 0.2 mm from the wall is affected. In contrast, cases (b) and (d) show these areas filled with particles, showing the seeder's good performance despite the low volume flow rates.

The images were further processed to quantify the apparent effect by applying a threshold-based

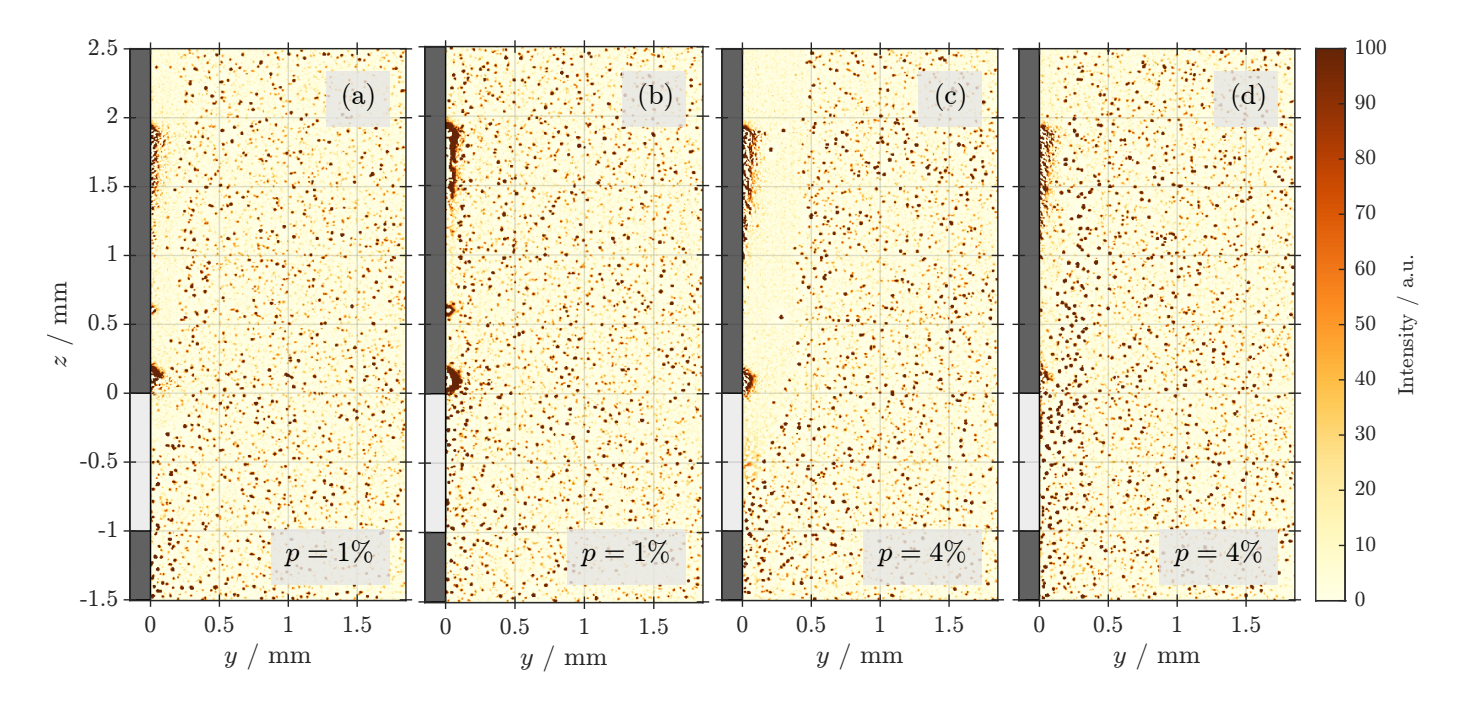
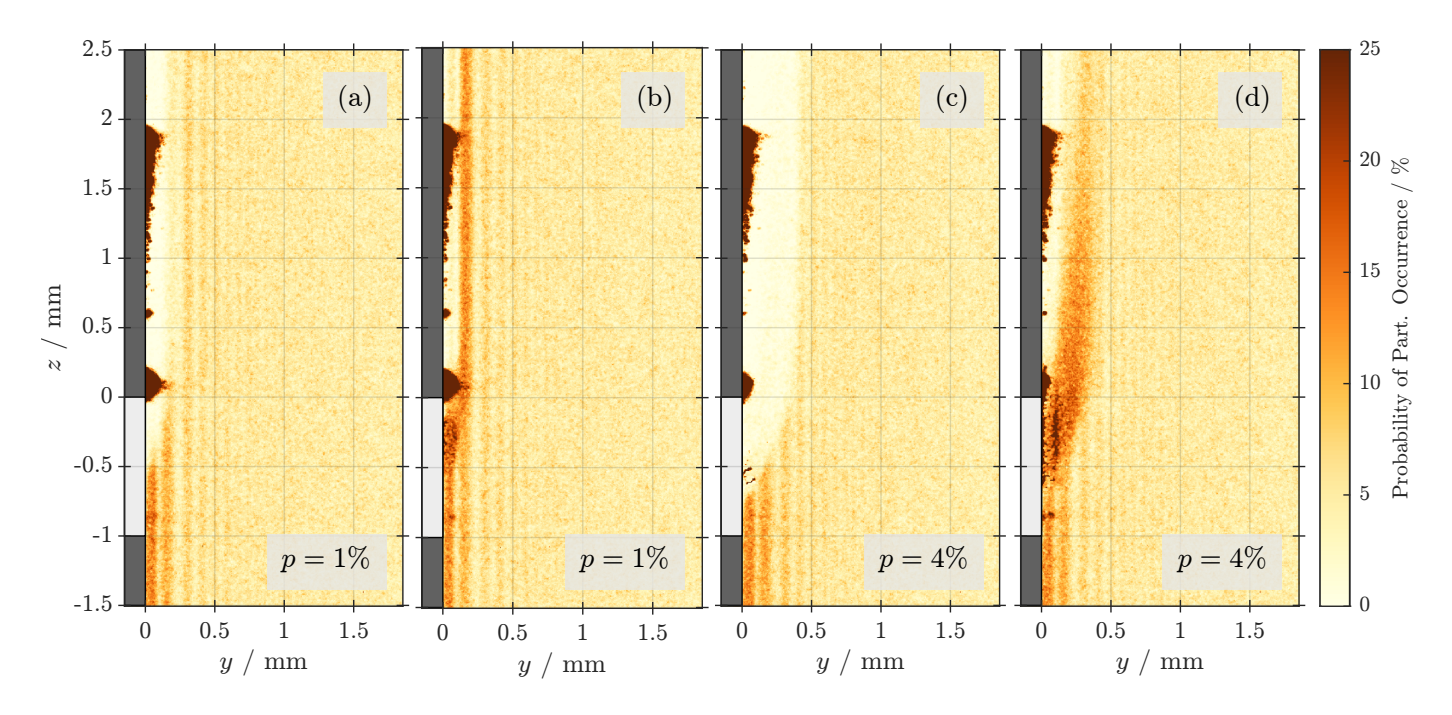


Figure 3. Processed Mie-scattering images of the seeded particles with the jet-flow from the bottom and the wall indicated in dark grey to the left. The jet flow is seeded in all images. The inlet in the wall is indicated in light grey from  $-1 \, mm$  to  $0 \, mm$ . (a) and (b) show  $1 \, \%$  mass flux per area from the wall-inlet in comparison to the main jet. In (c) and (d) the wall-inlet flow was increased to  $4 \, \%$ . The piezo-seeder for the wall inlet was turned off for (a) and (c), while active for case (b) and (d).

binarisation. The binarised images were then averaged to obtain a probability map showing the likelihood of finding a particle at a specific pixel, corresponding to a particular spatial location In Fig. 4. A pixel containing a particle in every recorded image corresponds to 100%, and a pixel without any single particle detected throughout all recorded images corresponds to 0% in this map of the probability of particle occurrence. This method provides a simple measure to qualitatively estimate the seeding density, although it is also slightly sensitive to variations in the apparent particle size.

Fig. 4 shows the map of the probability of particle occurrence. Averaging the images highlights the dewarped stripey noise pattern, which remains visible despite the thresholding. Nevertheless, the map of the probability of particle occurrence supports assessing the seeder performance. The jet shows a homogeneous probability of particle occurrence of just below 5% on average in all cases. Upstream of the wall-inlet, close to the wall, probability of particle occurrence appears to increase, with an average of 7%-10%, although this effect might be influenced by noise. The seeder's effect on the local seeding density is visible at and downstream of the wall-inlet. In cases (a) and (c), without the piezo-seeder in operation, the probability of particle occurrence in the area influenced by the inlet lowers to an average of about 1%. However, the seeder raises the probability of particle occurrence close to the wall, downstream the inlet, to an average of 7%-9%, which closely matches the average up to the same distance from the wall upstream of the inlet. Therefore, the piezo-



**Figure 4.** This map of probability of particle occurrence is obtained by binarising the image via a threshold and averaging. Cases and field of view are identical to Fig. 3.

based seeder is capable of providing a sufficient number of particles for PIV studies assessing the boundary flow conditions in this case. Further downstream, the probability of particle occurence close to the wall lowers to 3%-6% on average. This effect is likely due to the evaporation of the ethanol used to seed the inlet.

In the Mie-scattering shown in Fig. 3, the particles from the piezo-based seeder appear larger and with higher intensities than the particles in the vertically oriented main jet. To closer examine this observation, the binarisation of each frame was used as a mask, removing all intensity values besides the particles. Averaging the masked intensities usinf all 200 frames provides a measure of the average intensity of the particles without taking their probability of occurence into account, as this operation ignores the intensities when no particle is present. Fig. 5 shows the resulting averaged intensity fields. Case (d) shows that the particles from the wall-inlet appear to have a higher intensity than those in the jet while they are still close to the inlet. However, about 7 cm downstream, the particles from the jet are almost indistinguishable from the other particles from the jet. This suggests that the particles from the piezo-based seeder using ethanol are initially larger than the DEHS droplets in the jet. However, as the ethanol droplets evaporate fster than the DEHS droplets, downstream the wall inlet their size is likely comparable to the droplets in the jet. In case (c), the seeder was turned off minutes before the images were recorded, and the probability map in Fig. 4 showed very few particles in the region downstream from the inlet. However, based on Fig. 5, it appears that some few ethanol particles were still expelled from the seeder into the inlet, as indicated by the distinguishable large particles still visible after the averaging.

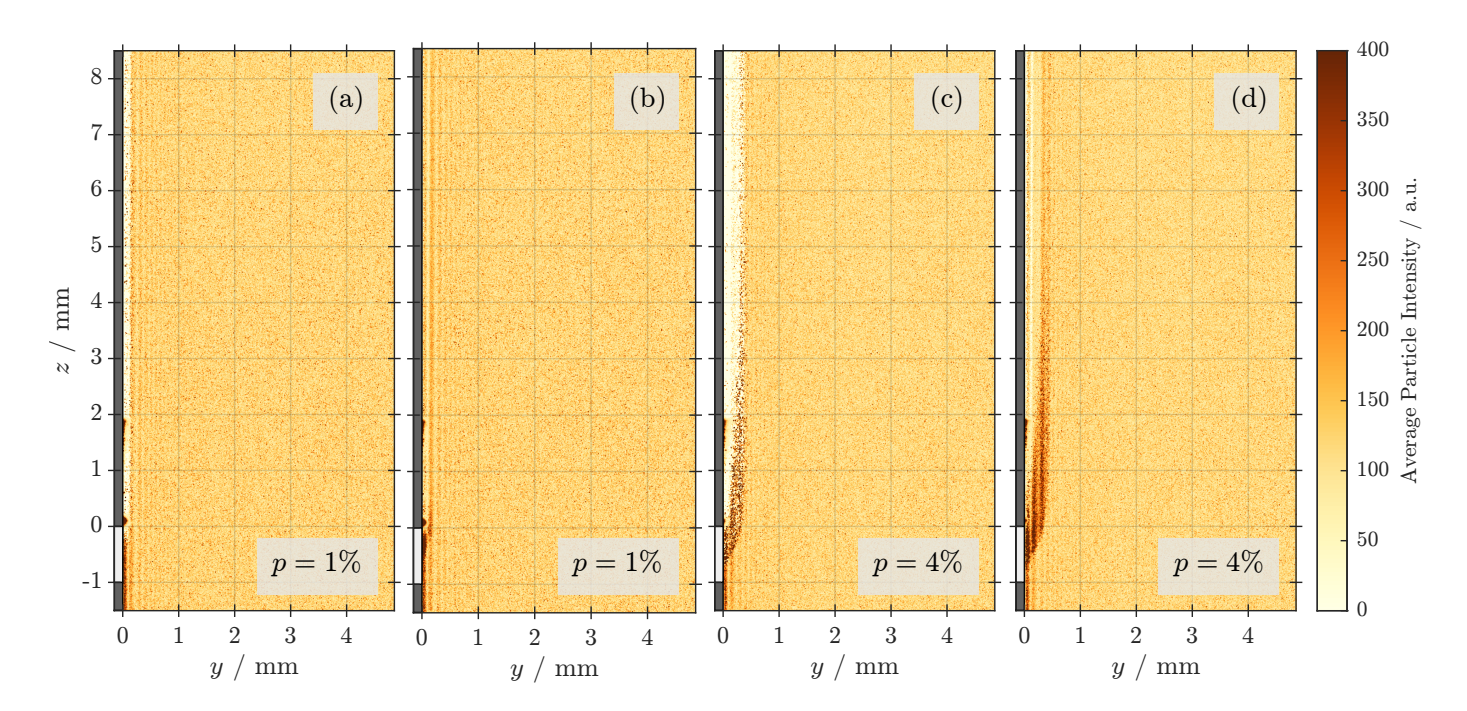


**Figure 5.** Intensity probability map calculated using a binarisation of the probability as a mask for the intensity and subsequent averaging. Cases are identical to those in Fig. 3, but with a larger field of view to display changes in particle intensities further downstream of the wall inlet. The high-intensity particles visible near the inlet in case (c) are likely due to insufficient flushing of the seeder, which is a result of the low volume flow rates.

In conclusion, the piezo-based seeder operated with ethanol appears to work well for the present application. It provides seeding through the low-volume flow wall inlet, resulting in comparable particle occurrence probabilities with sizes initially slightly larger than those from the conventional DEHS seeder used for the main jet.

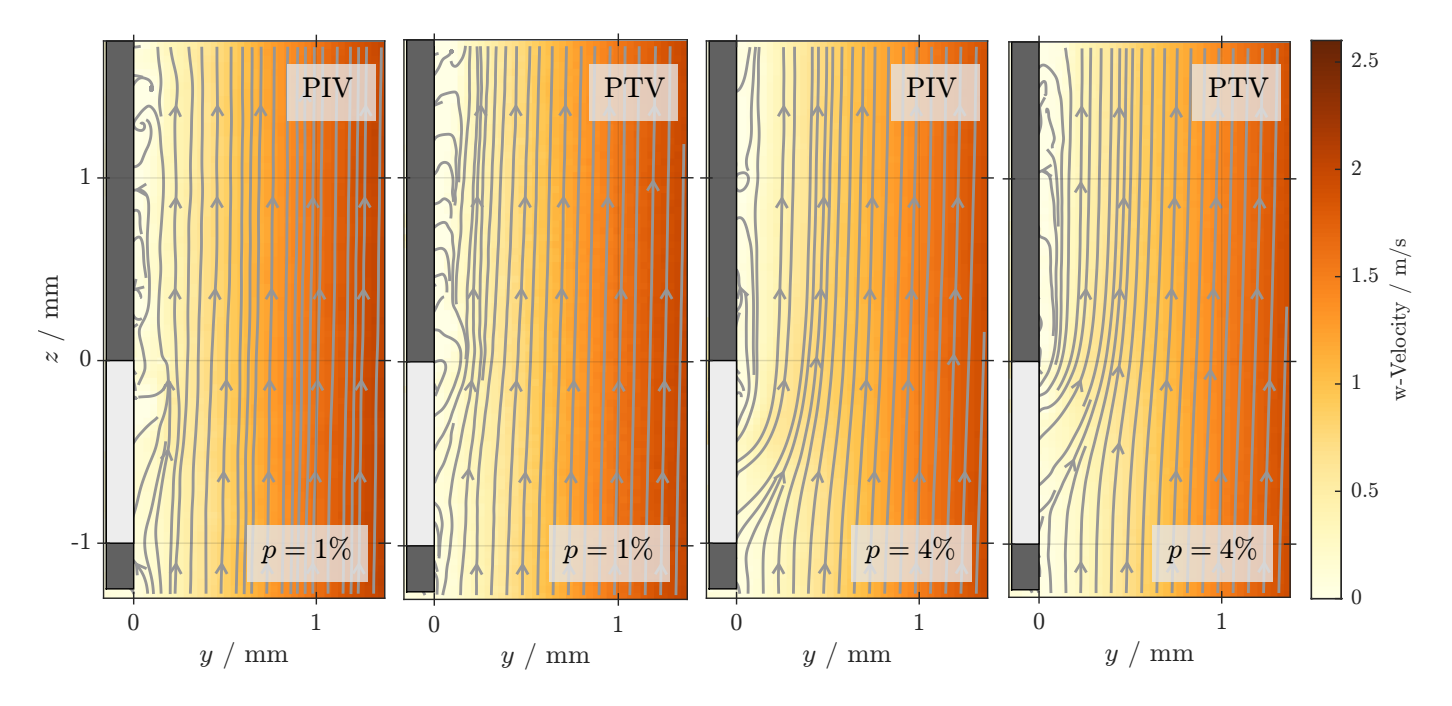
### 4.2. Flow Field Measurements

In this section, we present the flow field measurements using the novel seeder design. The cases with seeding from the wall inlet, specifically case (b) and case (d), were processed using Particle Image Velocimetry (PIV) and Particle Tracking Velocimetry from PIV (PTV from PIV) based on the PIV correlation using DaVis 10 software from LaVision GmbH.

The case with p=1% was evaluated with a time step (dt) of 20  $\mu$ s, resulting in a maximum pixel shift of 8  $\mu$ s. Near the wall, however, the pixel shift decreases significantly. For the case where p=4%, the dt was increased to 40  $\mu$ s.

Both cases were processed using interrogation windows of size  $24 \times 24 \,\mathrm{px}$  with 75% overlap. This setup corresponds to a velocity vector computed every 144 µm, resulting in a vector spacing of approximately 36 µm from the overlap. Only vectors with a correlation value greater than 0.6 were considered for evaluation.

PTV from PIV vectors were derived from the PIV correlation with a correlation window size of  $4\times4\,\mathrm{px}$  and an intensity threshold for particle detection of 30 counts. The resulting unstructured velocity data was binned into a  $6\times6$  pixel grid for all 200 recorded double images. The binning size was chosen to account for the typical particle size, which is 3-6 pixels. This binning ensures that the entire flow field statistically contains more than 90 particles per bin over all incorporated frames, while maintaining a vector spacing of 36  $\mu$ m without overlap.

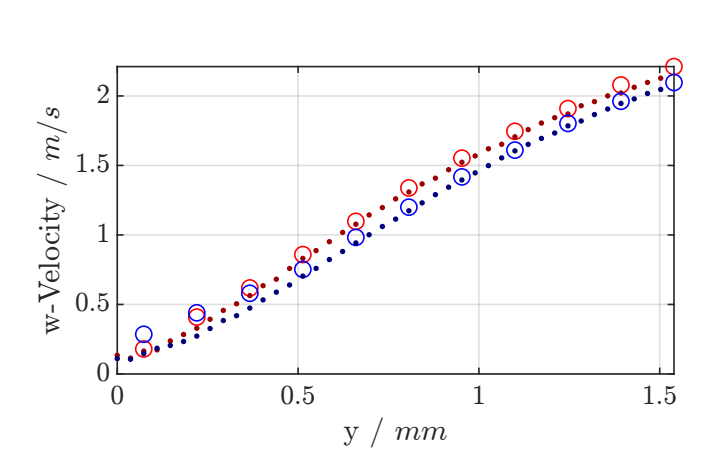


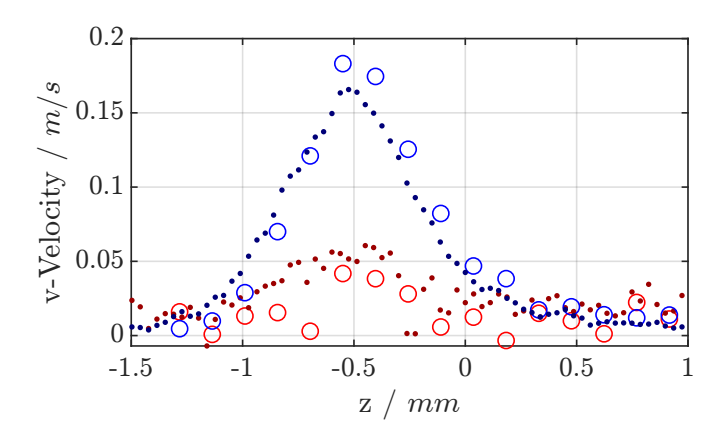
**Figure 6.** PIV results showing the w velocity field measured along the vertical wall for different flow rates (p = 1% and p = 4%). The left two panels show PIV results for p = 1% and p = 4%, while the right two panels show the corresponding PTV results. The color map indicates the w velocity in m/s, and the arrows represent the velocity vectors.

Figure 6 shows the PIV results showing the w velocity field measured along the vertical wall for different flow rates ( $p=1\,\%$  and  $p=4\,\%$ ). The left two panels show the PIV results for  $p=1\,\%$  and  $p=4\,\%$ , while the right two panels show the corresponding PTV from the PIV results. The color map indicates the w velocity in m/s, and the arrows represent the velocity streamlines.

Figure 7 shows the velocity profiles for w velocity (left) and v velocity (right) as a function of distance from the wall (y and z axes). Circles represent PIV measurements, while dots represent PTV from PIV measurements. These profiles highlight the differences in velocity distribution near the wall and further downstream, providing insight into the boundary layer evolution.

The two cases with wall inlet seeding (case (b) and case (d)) show different flow characteristics. For the case  $p=1\,\%$ , evaluated with a dt of 20 µs, the maximum pixel displacement was observed to be 8 px. Closer to the wall, the pixel shift decreased drastically. In contrast, the case  $p=4\,\%$  was evaluated with a larger dt of 40 µs.





**Figure 7.** Velocity profiles for w-velocity (left) and v-velocity (right) as a function of distance from the wall (y and z axes). Circles represent PIV measurements, while dots denote PTV measurements. Red dots represent p=1% and blue dots p=4%.

The processed PIV results, as shown in Figure 6, show the w velocity field with streamlines superimposed in the region near the wall inlet. The PTV from the PIV analysis provided additional insight, with a higher resolution of the velocity vectors due to the smaller correlation window and binning.

The velocity profiles in Figure 3 show the effect of the inlet flow on the boundary layer. The w velocity profile shows a gradual increase with distance from the wall, while the v velocity profile shows a peak near the inlet, indicating the influence of the seeding flow.

Figure 6 shows the resulting w-velocity with streamlines overlaid, in the region close to the wall inlet. The velocity gradient due to the wall is clearly visible, and the flow from the wall inlet is well resolved. In the p=4% case, the flow from the wall inlet pushes much further into the stream, with the streamlines from the top of the wall inlet maintaining some distance from the wall further downstream. This observation corresponds well to the streak of particles from the wall inlet visible in Figure 5.

Close to the wall, the velocities approach  $0 \,\mathrm{m/s}$ , which limits the meaningfulness of the streamlines in this region. To compare the results further, Figure 7 shows a wall-normal w-velocity profile 4 mm downstream from the inlet, as well as a wall-parallel u-velocity profile at a 0.25 mm distance from the wall.

The improved spatial resolution provided by PTV from PIV is clearly apparent in Figure 7, high-lighting its effectiveness in capturing detailed flow characteristics. These observations collectively highlight the dynamics of the boundary layer and the effectiveness of the seeder in resolving the intricate flow patterns near the wall inlet. The data underscore the importance of precise seeding in capturing the flow characteristics necessary for comprehensive evaluations in polymer combustion studies.

These observations collectively highlight the dynamics of the boundary layer and the effectiveness of the seeder in resolving the intricate flow patterns near the wall inlet. The data underscore the importance of precise seeding in capturing the flow characteristics necessary for comprehensive evaluations in polymer combustion studies.

### 5. Summary and Conclusions

In this study, we addressed the significant challenge of accurately seeding low-volume gas flows for high-resolution boundary layer velocimetry, which is essential for understanding polymer combustion and flame retardant effectiveness. Our work focused on the development and application of a novel piezo-based ultrasonic seeder capable of operating at extremely low flow rates and providing a steady supply of tracer particles necessary for Particle Image Velocimetry (PIV) and Particle Tracking Velocimetry from PIV (PTV from PIV) measurements.

The experimental setup mimicked the pyrolysis process in polymers using a vertical flame-wall interaction burner. We introduced fuel (CH<sub>4</sub>) through a small inlet in the wall to simulate the release of combustible gases. The main challenges included overcoming reflections from the wall and ensuring adequate seeding in the low volume flow relative to the main jet.

Our newly designed piezo-based ultrasonic seeder, using ethanol as the seeding liquid, demonstrated effective seeding at flow rates well below 2.579 L/h. The performance of the seeder was validated by PIV and PTV from PIV measurements, which showed significant improvements in spatial resolution and particle distribution near the wall inlet.

Flow field measurements revealed distinct velocity profiles for different seeding conditions, high-lighting the seeder's ability to maintain sufficient particle density in low volume flows. The results indicated that the seeder could provide detailed insight into boundary layer dynamics, which is critical for evaluating flame retardant performance.

Overall, the innovative seeder design proved to be effective in overcoming the limitations of conventional methods, enabling accurate and high-resolution velocimetry in low volume flow scenarios. This work provides a robust experimental foundation for future studies of polymer combustion and flame retardant effectiveness, and contributes valuable data for the advancement of fire safety research in polymeric materials.

Future work will focus on further refining the seeder design and exploring its application under reactive flow conditions. In addition, the integration of advanced image processing techniques can improve the accuracy and resolution of velocity measurements, providing deeper insights into the complex interactions within the boundary layer during polymer combustion.

# Acknowledgements

This work has been funded by the Deutsche Forschungsgemeinschaft (DFG, German Research Foundation) – Project Number 237267381 – TRR 150. Additionally, the authors would like to thank Brian Peterson and Alexander Nicolas from the University of Edinburgh for their support and input on processing methods.

### Nomenclature

- a Acceleration  $[m/s^2]$
- $A_i$  Area of the inlet [m<sup>2</sup>]
- $A_m$  Area of the main nozzle [m<sup>2</sup>]
- dt Time increment [µs]
- $\dot{m}_i$  Mass flux through the inlet [kg/s]
- $\dot{m}_m$  Mass flux through the main nozzle [kg/s]
- p Percentage of mass flux per area
- Re Reynolds number
- u Velocity component in the x-direction [m/s]
- v Velocity component in the y-direction [m/s]
- w Velocity component in the z-direction [m/s]
- *x* Coordinate in the x-direction [m]
- y Coordinate in the y-direction [m]
- z Coordinate in the z-direction [m]

#### References

Adrian, R. J., & Westerweel, J. (2011). *Particle image velocimetry* (Vol. 30). Cambridge: Cambridge Univ. Press.

Dasari, A., Yu, Z.-Z., Cai, G.-P., & Mai, Y.-W. (2013). Recent developments in the fire retardancy of polymeric materials. *Progress in Polymer Science*, *38*(9), 1357–1387. doi: 10.1016/j.progpolymsci .2013.06.006

Geschwindner, C., Goedderz, D., Li, T., Bender, J., Böhm, B., & Dreizler, A. (2023). The effects of various flame retardants on the combustion of polypropylene: Combining optical diagnostics and pyrolysis fragment analysis. *Polymer Degradation and Stability*, 211, 110321. doi: 10.1016/j.polymdegradstab.2023.110321

- Greifenstein, M., Zentgraf, F., Johe, P., Boehm, B., Steinhausen, M., Hasse, C., & Dreizler, A. (2024). Measurements of the local equivalence ratio and its impact on the thermochemical state in laminar partially premixed boundary layer flames. *Experiments in Fluids*, 65(1). doi: 10.1007/s00348-023-03747-z
- Haylett, D. R., Davidson, D. F., & Hanson, R. K. (2012). Second-generation aerosol shock tube: an improved design. *Shock Waves*, 22(6), 483–493. doi: 10.1007/s00193-012-0383-x
- Kurosawa, M., Watanabe, T., Futami, A., & Higuchi, T. (1995). Surface acoustic wave atomizer. *Sensors and Actuators A: Physical*, 50(1-2), 69–74. doi: 10.1016/0924-4247(96)80086-0
- Roudini, M., Patel, B., & Winkler, A. (2024). Developments for SAW-based aerosol generation: Miniaturized, cost-efficient, mass-producible, and reproducible systems. *Aerosol Science and Technology*, 1–12. doi: 10.1080/02786826.2024.2343377
- Schartel, B. (2021). *Plastics Flammability Handbook: The Burning of Plastics* (4th edition ed.). Carl Hanser Verlag GmbH & Company KG.
- Steinhausen, M., Ferraro, F., Schneider, M., Zentgraf, F., Greifenstein, M., Dreizler, A., ... Scholtissek, A. (2023). Effect of flame retardants on side-wall quenching of partially premixed laminar flames. *Proceedings of the Combustion Institute*, 39(3), 3745–3754. doi: 10.1016/j.proci.2022.07.207
- Velencoso, M. M., Battig, A., Markwart, J. C., Schartel, B., & Wurm, F. R. (2018). Molecular Firefighting-How Modern Phosphorus Chemistry Can Help Solve the Challenge of Flame Retardancy. *Angewandte Chemie (International ed. in English)*, 57(33), 10450–10467. doi: 10.1002/anie.201711735
- Wedding, J. B. (1975). Operational characteristics of the vibrating orifice aerosol generator. *Environmental Science & Technology*, 9(7), 673–674. doi: 10.1021/es60105a014
- Zentgraf, F. (2022). *Investigation of Reaction and Transport Phenomena during Flame-Wall Interaction Using Laser Diagnostics* (Doctoral dissertation). doi: 10.26083/TUPRINTS-00021314
- Zentgraf, F., Johe, P., Nicolas, A., Barlow, R. S., Böhm, B., Peterson, B., & Dreizler, A. (2024). On the evolution of turbulent boundary layers during flame—wall interaction investigated by highly resolved laser diagnostics. *Combustion and Flame*, 261, 113276. doi: 10.1016/j.combustflame.2023 .113276